Analytical Methods

PAPER

View Article Online
View Journal

Cite this: DOI: 10.1039/c8ay00241j

A ratiometric method for the oxidation mapping of metallic systems†

C. Gaviglio [a] and G. Carrone *[b]

In this work an imaging method used for studying metallic system oxidation is presented. This implementation monitors changes in the molecular absorption of visible light with a redox probe, a ruthenium polypyridine complex. As the transmission microscopy method avoids irradiation of the sample with high intensity light in comparison to fluorescence techniques, images can be acquired using an inexpensive commercial digital camera, making this an excellent low-cost tool for oxidation mapping. Molar fractions of reduced and oxidized species of the probe are calculated using different channels of an RGB camera, green and red, respectively, allowing a ratiometric measurement for redox potential determination with a high temporal and spatial resolution.

Received 31st January 2018
Accepted 5th April 2018

DOI: 10.1039/c8ay00241j

rsc.li/methods

Introduction

Imaging tools using molecular probes offer an opportunity to visualize and, even more interestingly, to quantify different parameters in diverse systems. Moreover the acquisition of images as a function of time allows studying diverse physical, chemical and biological processes.[1] Due to great advances in digital cameras, the use of imaging techniques has improved over the last few years, making these methods simple, efficient and inexpensive tools.

Fluorescent probes have been specially developed and are more commonly used in imaging methods.[2] Nevertheless a fluorescence-based system requires high intensity excitation light for sample irradiation which could deteriorate or induce photobleaching of the sample or the probe. Moreover, as fluorescent molecules emit in all directions only a fraction of the light emitted by the probe will be captured by the objective, making efficient and costly microscope objectives and expensive cameras necessary.

In order to overcome these disadvantages, optical transmission microscopy is a convenient alternative.[3] The amount of light needed is less in comparison to a fluorescent system as most of the light is transmitted by the objective and only a fraction is absorbed by the sample, and consequently the amount of light that reaches the detector is larger. This allows the use of low intensity excitation light for sample irradiation with a good signal/noise ratio and high spatial and temporal resolution in imaging acquisition. Therefore, the development of absorption probes is a challenge of great interest.

The choice of the appropriate molecular probe for imaging could allow the determination of different variables. For example, pH may be mapped using calcon as a pH indicator.[3] Ion concentrations and redox potential may also be mapped with suitable probes. In the case of redox potential determination, imaging techniques can be used to study many processes in biological systems[4] and other important redox processes such as corrosion in materials of different composition.[5]

Metallic materials (especially iron) are present in many objects of everyday use and corrosion processes have an important impact on economic and industrial processes, so different strategies such as modification of material properties or treatment of their surfaces with different types of inhibitors or coating with inorganic or organic materials have been developed to avoid or decrease corrosion.[6] Diverse techniques with high spatial resolution have been developed for monitoring corrosion processes based on different physical or physicochemical methods.[7] Many of them use electrochemical instrumentation, some examples to be mentioned are Electrochemical Impedance Spectroscopy (EIS), Local Electrochemical Impedance Spectroscopy (LEIS), Scanning Vibrating Electrode Technique (SVET), Scanning Kelvin Probe (SKP), Scanning Kelvin Probe Force Microscopy (SKPFM), and Scanning Electrochemical Microscopy (SECM) among others.[8] Although these techniques have good precision and exactitude they present the disadvantages of high cost and inability to map a large area at the same time in order to make a real time study of the process. In this sense it would be interesting to develop new robust, economic, and high spatial and temporal resolution methods for monitoring localized corrosion processes in microscopic systems.

[a]Comisión Nacional de Energía Atómica, CAC-GIyANN, Departamento de Física de la Materia Condensada, Avenida General Paz 1499, San Martín 1650, Buenos Aires, Argentina

[b]Departamento de Química Inorgánica, Analítica y Química Física, INQUIMAE, Facultad de Ciencias Exactas y Naturales, Universidad de Buenos Aires, Ciudad Universitaria, Pabellón 2, AR1428EHA Buenos Aires, Argentina. E-mail: carroneguillermo@gmail.com

† Electronic supplementary information (ESI) available. See DOI: 10.1039/c8ay00241j

In this work we present a low cost 2D imaging method for the oxidation mapping of different iron microscopic systems in real time and redox potential determination using a domestic digital camera coupled to a transmission microscope which senses a redox molecular probe (ruthenium complex). The use of a domestic digital camera to acquire images has several advantages besides its low cost, such as it provides a high spatial (millions of pixels where each one represents a value of the measurement) and temporal resolution (in the order of 1000 fps, frames per second) and allows ratiometric measurements to be done.

As these cameras are intended for domestic use, they are designed to emulate human vision. One of the simplest ways to obtain this is by dividing each pixel into a filter pattern (Bayer pattern, or RGB, R: red, G: green and B: blue), in which for every two G sensors there is one R sensor and one B sensor. This relationship between RGB channels has the disadvantage that R and B channels have a spatial resolution and sensitivity lower than those of the G channel, resulting in images with higher noise for those channels. To overcome this disadvantage an averaging procedure that accounts for this imbalance can be implemented. One important advantage of RGB sensors is that they allow the possibility of performing a measurement in which signals representing different species of a molecular probe are simultaneously detected by independent channels. In this case, the oxidized species of the redox probe is measured by one channel while the reduced species is measured by the other (*vide infra*).

Monitoring redox changes *via* this image acquisition method requires the use of a specific molecular probe whose absorption spectra of the reduced and oxidized species of the redox equilibrium have to be compatible with the RGB response channels of a digital camera, and consequently valuable information can be obtained through image processing.

A class of redox probes where both species satisfy the necessary condition to be measured by independent channels are ruthenium polypyridine complexes (Ru-pp). These ruthenium complexes are formed by coordination of two bidentate ligands (polypyridine) and, in most cases, also by two monodentate ligands to the metal center. Usually in these complexes Ru has an oxidation state of II or III and an $E^{o}_{Ru(III)/Ru(II)}$ of $\cong$ 1 V (*vs.* SHE, Standard Hydrogen Electrode) that can be modified by introducing changes in the coordinated ligands.[9,10] These compounds exhibit a quasi reversible redox process controlled by diffusion (ESI†). Different types of electronic transitions are involved in Ru-pp complexes[11] (MC, metal centered; LC, ligand centered; MLCT, metal to ligand charge transfer; LMCT, ligand to metal charge transfer). The relevant transitions of this family of compounds are MLCT (for the reduced species) and LMCT (for the oxidized species). The position of these absorption bands depends on the ligands coordinated to the metal center.[10,12] Even though this family of ruthenium(II) complexes is usually used for photoliberation of a ligand,[3,13] as the photodelivery quantum yield depends on the position of the MLCT band,[12] it is possible to design complexes where the photoliberation is sufficiently low ($\Phi \sim 10^{-2}$) and these probes are stable during the experimental time because of using low light intensity.

With this idea in mind, various ruthenium polypyridine complexes have been synthesized and their absorption properties have been compared, in order to fulfill the main requirement of the probe which comprises the overlap of the absorption bands of the reduced and oxidized species with the G (green) and R (red) channels of a digital camera, respectively, and the range in which the desired variable can be measured, in this case it is related to the standard reduction potential, E^{o}.

The strong influence of the ligands on the UV-vis absorption spectra of the different complexes is well known. The positions of the MLCT and the LMCT bands, previously mentioned, are related to the stabilization of the corresponding excited states.[12,14] Also E^{o} depends on the stabilization or destabilization of the Ru(III) species according to ligand modifications.[9,10]

Taking advantage of the versatility of this kind of probe, compounds that adapt as best as possible to the requirements of the method have been designed.

Experimental

Synthesis and characterization

Synthesis of metal complexes was carried out in the absence of light and under a nitrogen atmosphere unless otherwise indicated. All solvents were of reagent grade or better. Aqueous solutions were prepared with double deionized water (DDW) obtained from a Milli-Q purification system (Millipore, Bedford, MA, USA). Commercially available reagents were used as received. Synthetic procedures are described in the ESI.†

Cyclic voltammetry was carried out using a TEQ-03 potentiostat, a three-electrode configuration (Ag/AgCl, Sat. KCl reference electrode; Pt counter electrode; and glassy carbon, surface = 9.4 mm^2, as the working electrode), 0.1 mM complex and 0.1 M Na_2SO_4 in water. All the potentials are expressed against the SHE. The results are shown in the ESI.†

UV-vis spectra were acquired on a Hewlett-Packard HP8453 diode array spectrometer with a 1 cm path length cuvette.

^{1}H NMR spectra were recorded using a Bruker 500 MHz NMR spectrometer. ^{1}H NMR chemical shifts were referenced to the residual hydrogen signal of the deuterated solvent (2.05 ppm, acetone). Abbreviations used in the description of NMR data are as follows: br, broad; s, singlet; d, doublet; t, triplet.

Image acquisition setup

Images were acquired using an inverted Nikon TS-100 microscope with bright field illumination. The illumination system of the microscope was replaced with a two-LED set irradiating green (535 $\pm$ 16 nm fwhm) and red (635 $\pm$ 11 nm fwhm) light and aligned by a dichroic mirror, and resistors were connected in series which, together with a regulated voltage source, were used to obtain the same illumination intensity for both LEDs. In order to decrease possible irregular illumination from the LEDs and to favor a homogeneous illumination field of the sample, a homemade diaphragm was attached. With this irradiation system, one of the species of the redox probe absorbs red light

Fig. 1 Picture of the setup used as an interface for transmission measurements of different systems. (Left) (A) camera; (B) illumination system. (Right) Zoom picture of the illumination system (C) LEDs; (D) dichroic mirror; (E) homemade diaphragm.

and the other species absorbs the green one. The blue (B) channel of the digital camera is not used in the measurement so that it is available for any additional registration. Images were acquired using a conventional digital camera (Casio Exilim EX-FC100) which made focus through a normal eyepiece and a custom adapter and was set to ISO 100 sensitivity (a picture of the setup is shown in Fig. 1). Analysis of videos and images was done using public access ImageJ® software.[15] The image processing procedure is described in the ESI.† The corrosion monitoring experiment consists of immersion of an iron object in a 2 mM aqueous solution of the redox probe in the oxidized form. Previously the iron object was cleaned in 1 M HCl solution. Videos were filmed at 30 fps and are available in the ESI.†

Results and discussion

The redox probe selectivity depends on E^{o}, which must be near the potential range to be monitored. Therefore, ligand modifications of the ruthenium complexes were introduced in order to obtain different E^{o} values of the probes. Higher electron density donated to the metal ion by the ligands promotes a more negative reduction potential of the Ru(III)/Ru(II) couple.[9,10]

Cyclic voltammograms were obtained in aqueous solution at 100 mV s^{-1} scan rate for the different complexes (Fig. 2, inset) and their E^{o} values *vs.* SHE are presented in Table 1. All of them present a reversible redox process positioned at 750–900 mV *vs.* the SHE range depending on the ligands coordinated to the metallic center. A shift of 50 mV towards more negative potentials is observed when both monodentate ligands 4AP are replaced by DMAP. Moreover when both bidentate ligands bpy are replaced by 5,5′dmbpy a shift of −100 mV approximately is detected. These values are in agreement with the relation proposed by Lever *et al.*[9]

Also cyclic voltammetry of $[Ru(bpy)_2(4AP)_2]^{2+}$ was carried out at different scan rates (Fig. 2) resulting in a modification of the detected current and of the separation waves. The diffusion coefficient (D) was calculated using the Randles and Svecik equation[16] (2.14×10^{-6} cm^2 s^{-1}, in agreement with similar complexes[17]) and the calculated rate constant of electron transfer (k_o) was 5.34 10^{-3} cm s^{-1} (obtained using the quasi reversible reaction analysis of the one-step one electron process proposed by Matsuda–Y. Ayabe;[18] plots are shown in the ESI†). Although the measurement was done in a different system

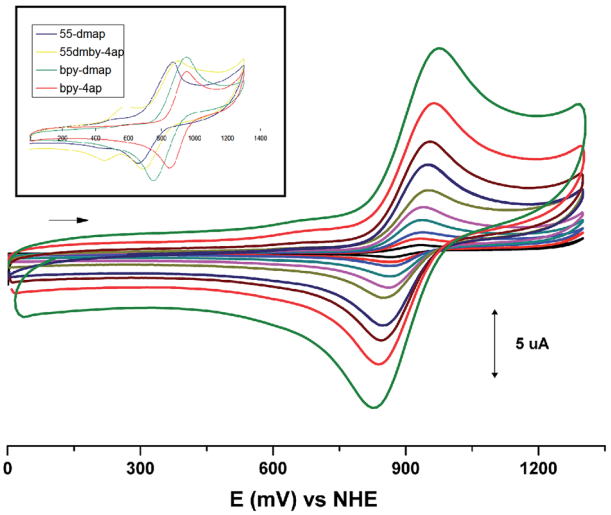

Fig. 2 Voltammograms of $[Ru(bpy)_2(4AP)_2]^{n+}$ at different scan rates. (Inset) Cyclic voltammograms of $[Ru(pp)_2(L)_2]^{n}$ complexes (blue: pp = 55′dmbpy, L = 4DMAP; yellow: pp = 55′dmbpy, L = 4AP; green: pp = bpy, L = 4DMAP; red: pp = bpy, L = 4AP). Scan rate: 1, 5, 10, 25, 50, 100, 200, 300, 500 and 1000 mV s^{-1}.

(carbon electrode), this parameter can be used to evaluate the rate and reversibility of the redox reaction of the probe.

This ligand modification of the coordination sphere of the metal also introduced changes in the absorption spectra of the redox probe species and compromised their compatibility with the RGB sensor. The overlap of the absorption bands, used in the measurement, with the channels of the camera must be maximized.

In order to exploit the versatility of complexes of the family $[Ru(pp)_2(L)_2]^{n+}$ (pp = polypyridine) as redox probes using the proposed method it is necessary to know how the visible range absorption spectrum is modified according to the nature of the coordinated ligands. The stabilization or destabilization of the excited state generates a dependence of the position of the MLCT (or LMCT) absorption band on the donor or acceptor nature of the ligands coordinated to the metal center.[12,14]

Absorption spectra of the synthesized ruthenium complexes are presented in Fig. 3 and their maximum absorption positions are summarized in Table 1. Absorption bands at low energy values correspond to the oxidized species (LMCT transition, $n = 3$) and those at high energy values correspond to the reduced species (MLCT transition, $n = 2$).

Table 1 E^{o} *vs.* SHE and UV-visible spectroscopic properties of the synthesized probes, $[Ru(pp)_2(L)_2]^{n+}$

			λ_{max} (nm)	
Pp	L	E^{o} (mV)	$n = 2$	$n = 3$
Bpy	4AP	903	486	745
Bpy	4DMAP	851	493	901
5,5′dmbpy	4AP	791	474	716
5,5′dmbpy	4DMAP	747	480	869

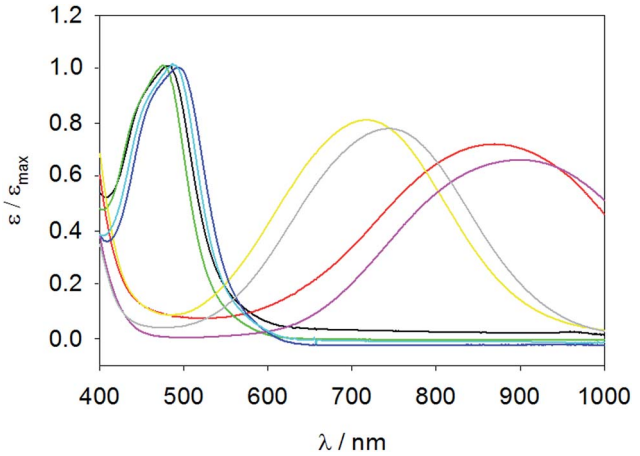

Fig. 3 UV-vis absorption spectra in aqueous solutions of $[Ru(pp)_2(L)_2]^{n+}$ pp = bpy, L = 4AP ($n = 2$, light blue; $n = 3$, gray); pp = bpy, L = 4DMAP ($n = 2$, blue; $n = 3$, pink); pp = 5,5′dmbpy, L = 4AP ($n = 2$, green; $n = 3$, yellow) and pp = 5,5′dmbpy, L = 4DMAP ($n = 2$, black; $n = 3$, red). All spectra are normalized regarding maximum absorption.

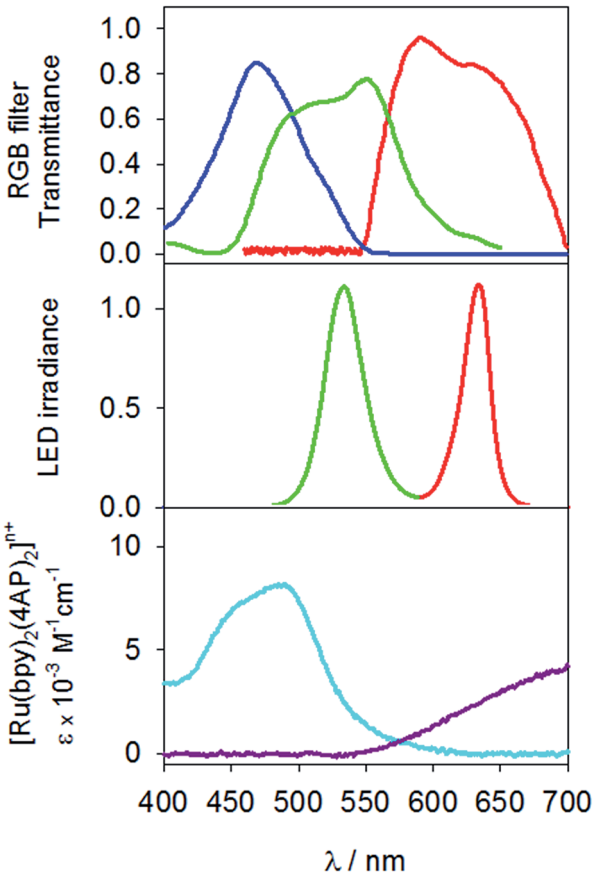

Fig. 4 RGB filter transmittances of the digital camera (top). Emission spectra of the LED illumination system (center). Absorption spectra of $[Ru(bpy)_2(4AP)_2]^{n+}$ (bottom), reduced species (light blue) and oxidized species (violet).

The reduced species of the molecular probe (where the MLCT band is involved in the measurement) with the 4DMAP ligand has a stronger donor effect in comparison to the 4AP ligand, favouring the stabilization of the excited state. Consequently the MLCT maximum absorption position of complexes with 4DMAP is shifted to higher wavelength, by more than 5 nm, with respect to complexes with 4AP. Although this effect increases the overlap between the absorption spectra of the complex in its reduced form and the G channel (Fig. 4 top) of the digital camera, the absorption band of the oxidized form (LMCT) is shifted to the IR region, where all the filters of the RGB sensors of the camera can transmit, not allowing an independent determination of the different species through the R and G sensors.

Therefore, another modification was introduced in the pp ligand in order to overcome this drawback. 5,5′dmbpy was used as a stronger donor ligand in comparison to bpy resulting in a shift of circa 30 nm to higher energies of the LMCT absorption band, increasing the overlap with the R channel (Fig. 4 top) of the camera. Although this modification favours absorption at 635 nm, it is still not high enough. Another disadvantage of the stronger donor 5,5′dmbpy ligand is that the MLCT absorption band in this complex is also shifted to higher energies due to a destabilization of the excited state, decreasing the overlap between the absorption spectra of the reduced species of the probe and the G channel of the camera.

Taking into account the absorption spectra of the different complexes and the illumination used to perform the measurements through the R and G channels of the camera, it was found that the molecular probe based on the complex $[Ru(bpy)_2(4AP)_2]^{n+}$ is the most suitable as a redox potential probe ($n = 2$ for the reduced form and $n = 3$ for the oxidized form). Absorption spectra of both species, reduced and oxidized forms, are compatible with the channels response of a digital camera. The G channel is used to measure the reduced form and the R channel is used to measure the oxidized one. Channel B (blue) is left free so that it is available for an additional measurement or for using a photochemical actuator. Due to the similar molar absorptivities of the reduced species at 535 nm and the oxidized species at 635 nm it is possible to use the dynamic range of the camera without saturation using similar illumination light intensity at those wavelengths. Fig. 4 (top) shows RGB filter transmittances of the digital camera, (center) emission spectra of the LED illumination system, and (bottom) absorption spectra of $[Ru(bpy)_2(4AP)_2]^{n+}$ ($n = 2$, light blue and $n = 3$, violet).

A schematic of the species involved in the measurement is presented in Fig. 5, Fe^0 oxidizes with the reduction of the Ru(III) complex. As these redox probes are not just indicators for iron corrosion (they intervene in the corrosion process as cathodic reagents, forcing iron to corrode) the corrosion rate will be proportional to their amount. In the case of studying natural corrosion, where the rate depends on O_2 and H_2O in the environment, another variable must be sensed (for example Fe^{2+}, the direct product of the iron oxidation half reaction) using the correct probe. The oxidation process of an iron pin submersed in an aqueous solution of the probe was followed in real time by imaging processing. Iron is oxidized and the ruthenium

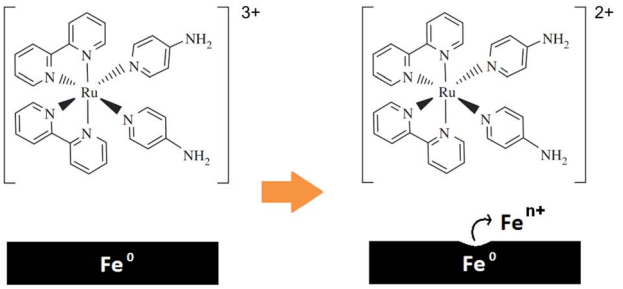

Fig. 5 Redox probe reduction and oxidation of the iron object in its exposed surface.

complex is reduced. The redox potential at each point of the system is calculated with the intensity values recorded during the measurement, considering the Lambert–Beer law and Nernst equation. Consequently the redox potential can be calculated from each pixel of the acquired image.

There are two possible methods for performing the measurement. On the one hand, as each species is measured using a specific channel, a channel can be used to calculate the molar fraction of the species and therefore the redox potential value for each pixel, using the Nernst equation. In this case the G channel was used because of its better resolution and X_R (molar fraction of the reduced species) was calculated. On the other hand, since this kind of probe has only two species in equilibrium (oxidized–reduced) a ratiometric measurement can be done using the R channel for measuring the oxidized species and the G channel can be used for measuring the reduced one, simultaneously. This type of measurement makes this a more robust technique.

The R channel has a lower signal/noise ratio than the G channel, due to the Bayer pattern of the channels of the camera. As a result, the R channel images are much noisier than G channel images, which hampers a direct use of a ratiometric G/R evaluation. The possibility of acquisition of many images in a short time allows an alternative to solve the problem described. One method to decrease the noise of the R channel is to take the average of several images considering the fact that the red sensor area is only half of that for the green channel. Although images were taken at a speed of 30 fps, when it is required, it is possible to use an image capture speed even two orders of magnitude higher (more than 1000 fps) with the same light intensity used in the experiment. Fig. 6 compares a processed image, representing the redox potential, using the ratiometric method (right) and using only G channel images (left). Histograms comparing data dispersion are shown in the ESI.†

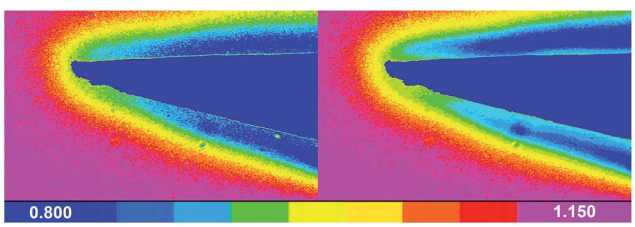

Fig. 6 Image representation of the redox potential using only the G channel (left) and the ratiometric method (right). Color scale represents redox potential (Volt) *vs.* SHE. Note: the colour of the metallic object was set by default by the image processing software, and it does not represent the redox potential, for more information see ESI.†

Selected RAW images (top) and the corresponding false color images (bottom) representing the redox potential value in each part of the system (iron pin) are presented in Fig. 7(a). In the first image, only green light is transmitted by the solution because the molar fraction of the reduced form of the probe (X_R) is null. With time the molecular probe is reduced near the metallic surface so X_R increases and the molar fraction of the oxidized probe (X_O) decreases. Consequently near the surface of the iron pin the transmittance at 535 nm decreases while at 635 nm a transmittance increase is observed. Throughout the experimental time, the diffusion process of the reduced probe is revealed by the increase of its absorption (535 nm) at locations more distant from the iron surface. As expected, a decrease of the concentration of the oxidized probe is observed near the iron surface, inducing a diffusion process of this species from the bulk of the solution to the iron surface. Therefore a redox potential gradient is produced in solution from the metallic surface to the bulk solution.

In order to inhibit the redox reaction in certain zones of the specimen its surface was partially masked with a varnish to avoid contact with the solution (ESI†), and the oxidation reaction only takes place in the unmasked region. In Fig. 7(b) RAW (top) and false color (bottom) images selected from the measurement are shown. As observed in the first images, the redox potential decreases near the exposed area but remains constant near the covered areas of the iron pin. Then the redox potential of the solution decreases due to the diffusion process of the probe.

The corrosion process of a smaller system in comparison with the first one, a commercial steel wool of 50 μm of diameter approximately, was followed in real time by imaging processing. Images are shown in the ESI.†

In order to determine the precision of the method, two techniques were employed for analyzing data dispersion in a selected image of the video measurement. In one case a line of 200 pixels length parallel to the metallic surface at a distance of 20 microns is analyzed at different times: 0, 5, 13, 20, 40 and 60 seconds (Fig. 8(a), line "x"). Considering that the redox potential remains constant, due to the shape of the surface and the probe diffusion, results should mostly differ due to the uncertainty of the method. Fig. 8(b) shows plots of redox potential values obtained in line "x" at different times of reaction. The results show that there is more dispersion for those values that are far from the redox probe E^o than for values closer to E^o. Plots of values obtained in a selected line from the image that is perpendicular to the specimen surface (Fig. 8(a), line "y") at times = 13, 20, 40 and 60 seconds show the same behavior and are shown in Fig. 8(c). Data dispersion was also analyzed through histograms obtained in selected areas (squares of 20 pixels length) where the redox potential is higher (A), similar (B) or lower (C) to E^o. Selected areas of the image are shown in Fig. 8(a) and the results

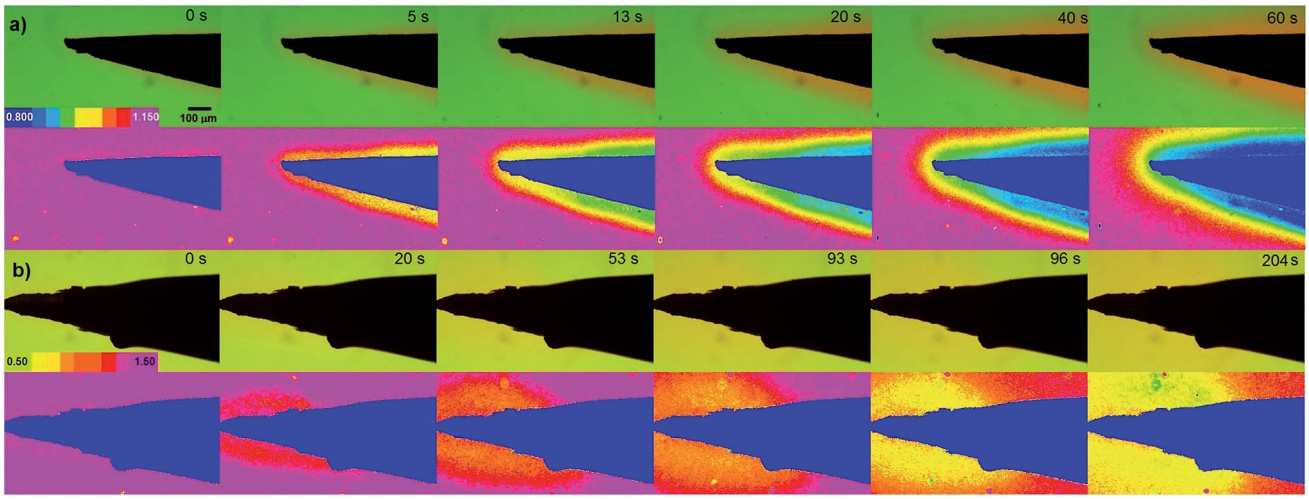

Fig. 7 (a) Selected images acquired at 30 fps for the oxidation process of the iron pin (t = 0, 5, 13, 20, 40 and 60 s). (Top) RAW images. (Bottom) False color images representing the redox potential obtained by the Nernst equation. (b) False color images representing the redox potential of selected images during the oxidation process of the iron pin with part of its surface covered by a varnish and the rest exposed to the solution where the reaction takes place (t = 0, 20, 53, 93, 96 and 204 s). (Top) RAW images. (Bottom) False color images representing the redox potential obtained by the Nernst equation. Note: colour scale represents redox potential (Volts) *vs.* SHE.

are presented in Fig. 8(d). Calculated values for the mean, standard deviation and ratio of the conjugated species of the redox molecular probe obtained from each selected area are summarized in Table 2. The same tendency is obtained with this analysis as the one observed in both regions near and perpendicular to the metallic surface.

Dispersion is lower for E values close to the redox probe E^o, where the concentration ratio of both species is equal to one, than for values farther from E^o, where the concentrations of both species are much different. Measurement error is mostly due to this reason.

An iron particle of 10 µm approximately, that detached from the iron pin during the experiment was analyzed with this methodology. The redox potential of the system is represented by a sequence of false color images (Fig. 9).

Analysis of calculated values was done for one of the images. Data dispersion of the redox potential values was analyzed through histograms obtained in selected areas (squares of 10 pixels length) presented in Fig. 10(a). Once more it can be confirmed that the standard deviation of E values is minimum near the E^o value. The deviations become nearly two orders of magnitude larger for potentials 200 mV above E^o than for potentials at which the ratio of oxidized/reduced species is almost one (Fig. 10(b)). Fig. 10(c) shows a plot of redox potential *vs.* position, in the direction across the iron particle. A redox potential gradient of *ca.* 200 mV across a distance of 15 µm can be observed.

A kinetic study of the oxidation reaction of the metallic system was done. An average of the measured values along lines of 200 pixels length parallel to the metallic surface and separated by 20 pixels between different lines was taken. Plots of the molar fraction of $[Ru(bpy)_2(4AP)_2]^{2+}$ (reduced species) *vs.* time for each line parallel to the surface are shown in Fig. 11,

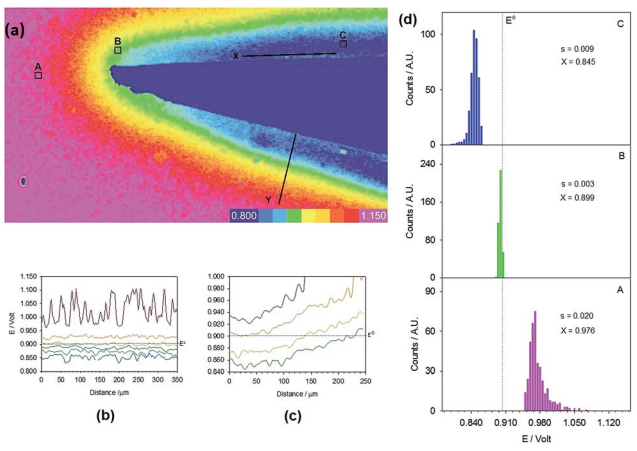

Fig. 8 (a) Selected areas of an image for analytical determinations. (b) Determination of the redox potential in a parallel direction with respect to the iron surface (line "x") at different times: 0, 5, 13, 20, 40 and 60 seconds. (c) Plots representing E *vs.* SHE as a function of time, obtained in a perpendicular line to the sample surface (line "y") at time = 13, 20, 40 and 60 s). (d) Histograms of the selected areas (A, B and C) obtained from squares of 20 pixels length (time = 60 s). Note: E^o refers to the standard redox potential of the probe and the colour scale represents redox potential (Volts) *vs.* SHE.

Table 2 Calculated values for the mean, standard deviation and ratio of the conjugated species of the redox sensor obtained from the analysis of histograms in Fig. 8

E^o (mV)	s (mV)	[ox]/[red]
845	9	0.105
899	3	0.855
976	20	17.27

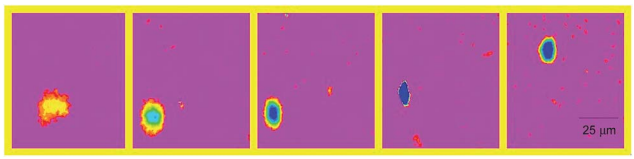

Fig. 9 False color images representing the redox potential of the corrosion process of an iron particle (of 10 μm approximately) selected from the acquired video (t = 0, 5, 13, 20, 40 and 60 s).

corresponding to the experiment of the iron pin with all the surface exposed to the redox probe solution.

As can be observed, the reduction of the probe in the oxidation process of the surface results in an increase of X_R in the area nearer to the surface as expected. At initial times a decrease in the rate of reduced probe production with increasing the distance from the metallic surface can be observed; and at larger distances the rate is almost null. This is due to the diffusion of the reduced probe from the metallic surface to the bulk solution. With time the diffusion process favors the increase of X_R in the bulk solution.

From the graphic of the nearer line to the metallic surface it can be observed that the oxidation of the metallic system by the Ru complex presents first order kinetics with an estimated rate constant of 1.0×10^{-2} s^{-1}. See ESI† for more details.

This kind of system, where the study of rate reactions involves the analysis in areas where the redox potential is far away from the E^o of the probe (where there is more measurement error), proves that the high spatial resolution of the method considerably decreases the uncertainty, as an average of hundreds of values can be taken.

Even though this method performs an analytical analysis with a high spatial and temporal resolution through a ratiometric measurement of the redox probe, this particular probe (designed in order to maximize the compatibility with the RGB channels) has a high E^o value which is not appropriate for studying natural corrosion, where O_2 and H_2O species are involved. For this case or other systems with this similar problem there are two possible alternatives for using this imaging method. One option would be to do the measurement with a probe with a more negative E^o, that maintains the compatibility with the RGB channels or resign this maximization (or even discard a ratiometric measurement and perform a one channel measurement), so the reduction of the probe by the metallic surface will not compete with the studied reaction. The other alternative, in order not to depend on the concentrations of the conjugated species of the redox probe, would be to use this economic method of image acquisition with high spatial and temporal resolution to sense another variable that depends directly on the reaction, considering its compatibility with the camera channels. With these modifications, the changes in the conjugated species of the probe would be only by the progress of the reaction to be studied instead of the reaction of the probe with the object.

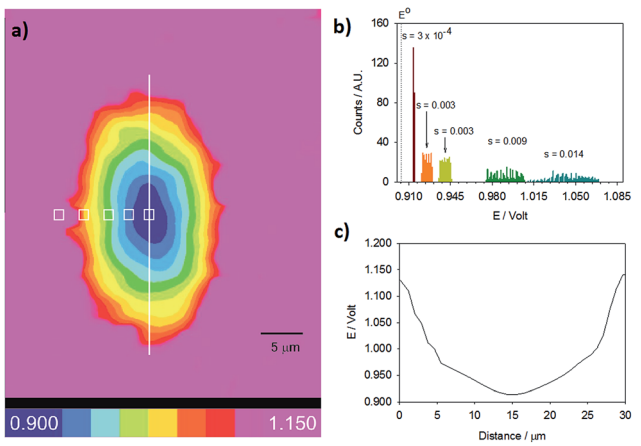

Fig. 10 (a) Enlarged image selected from Fig. 6. (b) Histograms of the selected areas obtained from squares of 10 pixels length; data dispersion increases for values not near to E^o. (c) Plot of redox potential *vs.* position, in the direction shown in (a). Note: colour scale represents redox potential (Volts) *vs.* SHE.

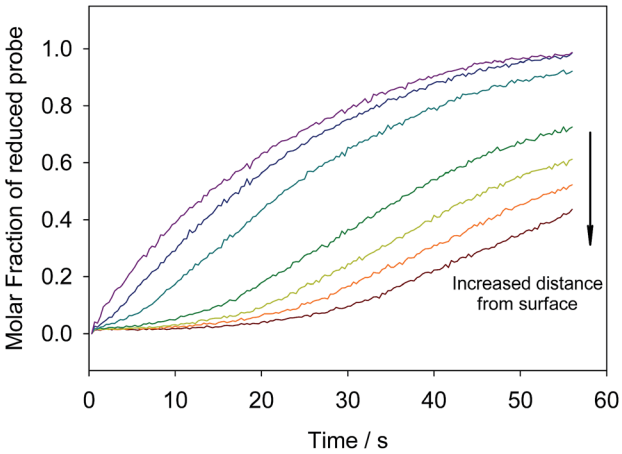

Fig. 11 Plots representing average values of the molar fraction of the reduced species of the probe (X_R), obtained along lines of 200 pixels length parallel to the metallic surface and separated by 20 pixels, *vs.* time obtained in the experiment shown in Fig. 8.

To extend the proposed method for measuring corrosion on top of a surface rather than on an edge, one option could be the modification of the illumination system, using reflection instead of transmission of light. In this way this method can be an excellent tool for studying materials, coatings or properties in order to avoid corrosion processes. Interestingly other systems can be monitored by this methodology using the appropriate redox molecular probe according to the needed E^o value. On the other hand, given the inexpensive and simple measurement methodology presented here, it is important to highlight the possible application of this work not only in research but also in different chemistry courses (inorganic, analytical, and photochemistry).

Conclusions

In this work, an inexpensive real-time imaging method for measuring the redox potential based on the absorption of light

by a redox probe, a Ru complex, is presented. This method was used for studying the redox process on iron material surfaces of different objects and can be expanded to other systems using different redox molecular probes. The use of a conventional digital camera as a tool for image acquisition allows this technique to have a high spatial and temporal resolution at a very low cost. Unlike fluorescence techniques, the type of illumination used by this technique increases the signal/noise ratio despite using a lower amount of light to illuminate the sample. This less intensity radiation used in the proposed method decreases both the possibility of photobleaching of the probe and the damage of the sample to be studied. Even though noise is higher for the R channel, due to the Bayer pattern of the RGB sensors of the camera, an average of a set of frames can be taken for reducing noise, and a ratiometric measurement can be done, making this method more robust. The precision of this method increases for redox potential values nearer to E^{o} of the probe that can be modified by introducing ligand modifications on the coordinated sphere of the Ru complex. With this method several redox probes, not only organometallic complexes, with different values of E^{o} can be used as long as the absorption spectra of the reduced and oxidized forms remain compatible with the sensors of the camera used to acquire the images. A perspective of great interest of these types of probes is that they can be used for studying iron surfaces through reflection microscopy techniques allowing the determination of oxidation process mapping on surfaces.

Conflicts of interest

There are no conflics to declare.

Acknowledgements

This research was supported by the National Agency for Science and Technology Promotion, CONICET, and University of Buenos Aires. CG and GC are members of CONICET.

Notes and references

1 (*a*) B. B. Kirby, N. Takada, A. J. Latimer, J. Shin, T. J. Carney, R. N. Kelsh and B. Appel, *Nat. Neurosci.*, 2006, **9**(12), 1506; (*b*) J. Ellenberq, J. Lippincott-Schwartz and J. F. Presley, *Trends Cell Biol.*, 1999, **9**(2), 52; (*c*) C. Gendrin, Y. Roggo, C. Spiegel and C. Collect, *Eur. J. Pharm. Biopharm.*, 2008, **68**, 828; (*d*) P. Bedner, H. Niessen, B. Odermatt, M. Kretz, K. Willecke and H. Harz, *J. Biol. Chem.*, 2006, **281**(10), 6673; (*e*) L. Bouffier, T. Doneux, B. Goudeau and A. Kuhn, *Anal. Chem.*, 2014, **86**, 3708.

2 (*a*) C. Wu, B. Bull, C. Szymanski, K. Christensen and J. McNeill, *ACS Nano*, 2008, **2**(11), 2415; (*b*) L. Yuan, W. Lin, K. Zheng, L. He and W. Huang, *Chem. Soc. Rev.*, 2013, **42**, 622; (*c*) C. Xu, R. M. Williams, W. Zipfel and W. W. Webb, *Bioimaging*, 1996, **4**, 198; (*d*) J. V. Frangioni, *Curr. Opin. Chem. Biol.*, 2003, **7**, 626.

3 O. Filevich, G. Carrone, V. Andino Pavlovsky and R. Etchenique, *Anal. Chem.*, 2012, **84**(13), 5618.

4 (*a*) R. M. Davis, A. L. Sowers, W. DeGraff, M. Bernardo, A. Thetford, M. C. Krishna and J. B. Mitchell, *Free Radical Biol. Med.*, 2011, **51**(3), 780; (*b*) M. Gutscher, A. L. Pauleau, L. Marty, T. Brach, G. H. Wabnitz, Y. Samstag, A. J. Meyer and T. P. Dick, *Nat. Methods*, 2008, **5**, 553; (*c*) H. Eto, F. Hyodo, N. Kosem, R. Kobayashi, K. Yasukawa, M. Nakao, M. Nikiwa and H. Utsumi, *Free Radical Biol. Med.*, 2015, **89**, 1097.

5 (*a*) Y. Yang, F. Scenini and M. Curioni, *Electrochim. Acta*, 2016, **198**, 174; (*b*) G. Williams, H. N. McMurray, D. Haymana and P. C. Morgan, *PhysChemComm*, 2001, **6**, 1; (*c*) S. R. Street, N. Mi, A. J. M. C. Cook, H. B. Mohammed-Ali, L. Guo, T. Rayment and A. J. Davenport, *Faraday Discuss.*, 2015, **180**, 251; (*d*) J. Passaretti Filho, M. A. Gomes Valente Jr, P. C. F. de Lima Gomes, C. S. Fugivara and A. A. Cardoso, *Anal. Methods*, 2017, **9**, 665.

6 (*a*) M. F. Montemor, *Surf. Coat. Technol.*, 2014, **258**, 17; (*b*) M. Ates, *J. Adhes. Sci. Technol.*, 2016, **30**(14), 1510; (*c*) V. Cicek, *Corrosion Engineering and Cathodic Protection Handbook: With an Extensive Question and Answer Section*, John Wiley & Sons, 2017; (*d*) H. H. Uhlig, *Uhlig's Corrosion Handbook*, John Wiley & Sons, 2011, vol. 51; (*e*) A. S. H. Makhlouf, *Handbook of Smart Coatings for Materials Protection*, no. 64, Elsevier, 2014.

7 P. Marcus and F. Mansfeld, *Analytical Methods in Corrosion Science and Engineering*, CRC Press, NY, 2006.

8 (*a*) A. Amirudin and D. Thieny, *Prog. Org. Coat.*, 1995, **26**, 1; (*b*) V. M. Huang, S. L. Wu, M. E. Orazem, N. Pébère, B. Tribollet and V. Vivier, *Electrochim. Acta*, 2011, **56**(23), 8048; (*c*) A. C. Bastos, M. C. Quevedo, O. V. Karavai and M. G. S. Ferreira, *J. Electrochem. Soc.*, 2017, **164**(14), 973; (*d*) M. Rohwerder and F. Turcu, *Electrochim. Acta*, 2007, **53**, 290; (*e*) D. E. Tallman and M. B. Jensen, Applications of Scanning Electrochemical Microscopy in Corrosion Research, in *Scanning Electrochemical Microscopy*, ed. A. J. Bard and M. V. Mirkin, CRC Press, 2012, pp. 451–488; (*f*) N. A. Payne, L. I. Stephens and J. Mauzeroll, *Corrosion*, 2017, **73**(7), 759.

9 A. B. P. Lever, *Inorg. Chem.*, 1990, **29**(6), 1271.

10 E. S. Dodsworth and A. B. P. Lever, *Chem. Phys. Lett.*, 1986, **124**(2), 152.

11 (*a*) K. Kalyanasundaram, *Coord. Chem. Rev.*, 1982, **46**, 159; (*b*) B. P. Sullivan, D. J. Salmon and T. J. Meyer, *Inorg. Chem.*, 1978, **17**(12), 3334.

12 D. V. Pinnick and B. Durham, *Inorg. Chem.*, 1984, **23**(10), 1440.

13 (*a*) A. Bahreman, J. A. Cuello-Garibo and S. Bonnet, *Dalton Trans.*, 2014, **43**(11), 4494; (*b*) L. Zayat, O. Filevich, L. M. Baraldo and R. Etchenique, *Struct. Bonding*, 2015, **165**, 47; (*c*) J. K. White, R. H. Schmehl and C. Turro, *Inorg. Chim. Acta*, 2017, **454**, 7; (*d*) G. Carrone and R. Etchenique, *Anal. Chem.*, 2015, **87**(8), 4363; (*e*) J. A. Cuello-Garibo, M. S. Meijer and S. Bonnet, *Chem. Commun.*, 2017, **53**, 6768; (*f*) G. Carrone, J. Pellegrino and F. Doctorovich, *Chem. Commun.*, 2017, **53**, 5314; (*g*) L. N. Lameijer, D. Ernst, S. L. Hopkins, M. S. Meijer, S. H. Askes, S. E. Le Dévédec and S. Bonnet, *Angew. Chem., Int. Ed.*, 2017,

56(38), 11549; (*h*) T. Respondek, R. Sharma, M. K. Herroon, R. N. Garner, J. D. Knoll, E. Cueny and J. J. Kodanko, *ChemMedChem*, 2014, **9**(6), 1306; (*i*) M. Huisman, J. K. White, V. G. Lewalski, I. Podgorski, C. Turro and J. J. Kodanko, *Chem. Commun.*, 2016, **52**(85), 12590.

14 K. Kalyanasundaram, S. M. Zakeeruddin and M. K. Nazeeruddin, *Coord. Chem. Rev.*, 1994, **132**, 259; M. K. Nazeeruddin, S. M. Zakeeruddin and K. Kalyanasundaram, *J. Phys. Chem.*, 1993, **97**(38), 9607.

15 C. A. Schneider, W. S. Rasband and K. W. Eliceiri, *Nat. Methods*, 2012, **9**(7), 671.

16 A. J. Bard and L. R. Faulkner, *Electrochemical Methods: Fundamentals and Applications*, John Wiley and Sons, USA, 2nd edn, 2000.

17 H. Ikeuchi, K. Naganuma, M. Ichikawa, H. Ozawa, T. Ino, M. Sato, H. Yonezawa, S. Mukaida, A. Yamamoto and T. Hashimoto, *J. Solution Chem.*, 2007, **36**(10), 1243.

18 (*a*) H. Matsuda and Y. Ayabe, *Bull. Chem. Soc. Jpn.*, 1955, **28**(6), 422; (*b*) H. Matsuda and Y. Ayabe, *Ber. Bunsenges. Phys. Chem.*, 1955, **59**(6), 494; (*c*) R. S. Nicholson, *Anal. Chem.*, 1965, **37**(11), 1351; (*d*) R. J. Taylor and A. A. Humffray, *J. Electroanal. Chem.*, 1973, **42**, 347.